JACS
JOURNAL OF THE AMERICAN CHEMICAL SOCIETY
Article
pubs.acs.org/JACS

In situ Cobalt–Cobalt Oxide/N-Doped Carbon Hybrids As Superior Bifunctional Electrocatalysts for Hydrogen and Oxygen Evolution

Haiyan Jin, Jing Wang, Diefeng Su, Zhongzhe Wei, Zhenfeng Pang, and Yong Wang*

Advanced Materials and Catalysis Group, ZJU-NHU United R&D Center, Center for Chemistry of High-Performance and Novel Materials, Key Lab of Applied Chemistry of Zhejiang Province, Department of Chemistry, Zhejiang University, Hangzhou 310028, P. R. China

Supporting Information

ABSTRACT: Remarkable hydrogen evolution reaction (HER) or superior oxygen evolution reaction (OER) catalyst has been applied in water splitting, however, utilizing a bifunctional catalyst for simultaneously generating H_2 and O_2 is still a challenging issue, which is crucial for improving the overall efficiency of water electrolysis. Herein, inspired by the superiority of carbon conductivity, the propitious H atom binding energy of metallic cobalt, and better OER activity of cobalt oxide, we synthesized cobalt–cobalt oxide/N-doped carbon hybrids (CoO_x@CN) composed of Co^0, CoO, Co_3O_4 applied to HER and OER by simple one-pot thermal treatment method. CoO_x@CN exhibited a small onset potential of 85 mV, low charge-transfer resistance (41 Ω), and considerable stability for HER. Electrocatalytic experiments further indicated the better performance of CoO_x@CN for HER can be attributed to the high conductivity of carbon, the synergistic effect of metallic cobalt and cobalt oxide, the stability of carbon-encapsulated Co nanoparticles, and the introduction of electron-rich nitrogen. In addition, when used as catalysts of OER, the CoO_x@CN hybrids required 0.26 V overpotential for a current density of 10 mA cm^{-2}, which is comparable even superior to many other non-noble metal catalysts. More importantly, an alkaline electrolyzer that approached ~20 mA cm^{-2} at a voltage of 1.55 V was fabricated by applying CoO_x@CN as cathode and anode electrocatalyst, which opened new possibilities for exploring overall water splitting catalysts.

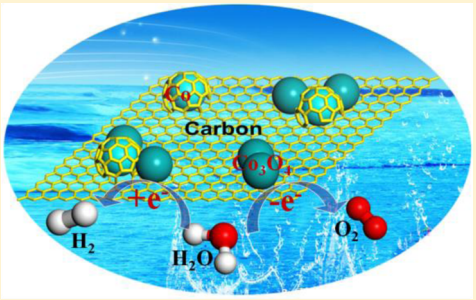

INTRODUCTION

Splitting water into hydrogen and oxygen to store light or electric energy in the form of chemical bonds has stimulated intense research due to accelerated depletion of fossil fuels.[1−5] The water-splitting reaction can be divided into two half-reactions: the hydrogen evolution reaction (HER) and the oxygen evolution reaction (OER), both of which are crucial for the overall efficiency of water splitting.[6−8] To increase the reaction rate and lower the overpotential, many superior catalysts have been explored toward HER and OER.[9,10] Currently, state-of-the-art hydrogen evolution catalysts consist of platinum-based materials.[11−13] However, the widespread application of Pt is limited by its scarcity and high cost, and thus the development of non-noble metal, metal composites, and even metal-free electrocatalysts[14,15] remains a crucial task. Such alternatives typically include MoS_2,[16−21] MoC,[22−24] WS_2,[25] NiMoN,[26] C_3N_4,[27] C_3N_4@NG,[28] etc., which function well in acidic media, but underperform in alkaline electrolyte. Generating hydrogen by electrolysis in alkaline media has been utilized for a number of years,[29,30] and it also offers high purity hydrogen (nearly 100%) for a moderate energy input.[31] Moreover, many catalysts present superior catalytic activity for OER in basic solution,[32,33] it is imperative to explore highly efficient HER catalysts in alkaline media to achieve the overall alkaline water electrolysis. As previously reported, metal Co has been calculated to have a low energy barrier for H adsorption,[34−37] thus Co-based composites may be promising catalysts for HER. Actually, many Co-based materials have been designed to catalyze the HER, including, for example, Co-NCNT,[38] CoP_4N_2,[39] cobalt corrole,[40] Co-coordination compound.[41,42] However, these catalysts always face the unsatisfactory catalytic properties for HER, thus it is highly necessary to design efficient Co-based catalysts for electrocatalytic hydrogen production. To realize the overall water splitting, highly active OER catalysts also need to be developed. It has been reported that compounds of earth-abundant cobalt (for example Co_3O_4) perform better toward OER.[43−48] However, the easy accumulation and low conductivity of pure Co_3O_4 decrease the active sites and hamper the transport of electrons or protons during the oxidation process.[49−52] In contrast, porous carbon support with high electric conductivity, large surface area,[53−55] structural flexibility[56] and strong tolerance to acid/alkaline environments is technically desirable to derive advanced Co-based hybrid catalysts.[57−59] Therefore, the combination of cobalt oxide and carbon can be excellent catalysts for OER, such as Co_3O_4/N-rmGO,[60] CoO-N-CG,[46] ZnCo-LDH,[61] NG-NiCo,[62] etc.

Despite that remarkable HER or superior OER catalysts can be applied in water splitting, utilizing a bifunctional catalyst for

Received: December 15, 2014
Published: February 6, 2015

DOI: 10.1021/ja5127165
J. Am. Chem. Soc. 2015, 137, 2688−2694

O_2 evolution and H_2 generation is still a challenging issue and scarcely reported, which is a crucial thought for designing overall water splitting catalysts.[63,64] Herein, inspired by the superiority of carbon, the low H atom binding energy of metallic cobalt, and better OER activity of cobalt oxide, we synthesized cobalt−cobalt oxide/N-doped carbon hybrids (CoO_x@CN) simultaneously applied to HER and OER by simple one-pot thermal treatment method. CoO_x@CN exhibited a small onset potential of 85 mV and low HER overpotential 235 mV to reach a current density of 10 mA cm^{-2} in 1 M KOH solution. Moreover, it also offered low charge-transfer resistance (41 Ω) and considerable stability for HER. Electrocatalytic experiments further indicated the better performance of CoO_x@CN for HER mainly origined from the high conductivity of carbon, the synergistic effect of metallic cobalt and cobalt oxide, the stability of carbon encapsulated Co nanoparticles (NPs), and the introduction of electron-rich nitrogen. In addition, when used as non-noble-metal catalysts of OER, the CoO_x@CN hybrids required 0.26 V overpotential for a current density of 10 mA cm^{-2}. Impressively, the catalytic activity of CoO_x@CN for OER remarkably improved after operating a hydrogen production reaction for 30 min, which was attributed to the improvement of the percentage of Co^{2+}. More importantly, an alkaline electrolyzer that approached ∼20 mA cm^{-2} at a voltage of 1.55 V was fabricated by applying CoO_x@CN as cathode and anode electrocatalyst, which brought us a new idea for designing overall water splitting catalysts.

EXPERIMENTAL SECTION

Materials. Melamine (M), D(+)-glucosamine hydrochloride (NG), glucose (G), cobalt(II) nitrate hexahydrate ($CoNO_3{\cdot}6H_2O$), potassium hydroxide (KOH), 5 wt % Nafion 117 solution, cobalt (II, III) oxide (Co_3O_4, 99.99% metals), cobalt (II) oxide (CoO, 99.99% metals), and cobalt (99.99% metals) were purchased from Aladdin. Commercial active carbon (AC) was gifted by ZHEJIANG NHU CO., Ltd. All were used as received without further purification.

Synthesis of Materials. The synthesis of CoO_x@CN was depicted in Scheme S1. Melamine (40 g) was mixed with cobalt(II) nitrate hexahydrate ($CoNO_3{\cdot}6H_2O$) (0.95 g), D(+)-glucosamine hydrochloride (1 g), and 400 mL water, then the homogeneous mixture was heated at 80 °C in an oil bath upon stirring overnight to remove the water. After that the dry mixture was grinded finely. The homogeneous compound was placed in the crucible and calcined at 600 °C in a type furnace for 1 h in N_2 atmosphere. The parent material placed was further raised to 800 °C at a ramp of 2.5 °C min^{-1} and kept at 800 °C for 1 h in N_2 atmosphere. For comparative studies and to obtain some insights into the structure electrocatalytic activity relationships of CoO_x@CN, more samples were prepared in N_2 atmosphere. The preparation of CoO_x@AC was similar to CoO_x@CN, except that the original materials were active carbon and $CoNO_3{\cdot}6H_2O$. CoO_x@C (non-nitrogen) was synthesized by applying glucose as carbon source, similar to CoO_x@CN. Furthermore, the fabrication of CN (melamine and D(+)-glucosamine hydrochloride as feedstock without $CoNO_3{\cdot}6H_2O$) was the same as CoO_x@CN, except the raw materials. After CoO_x@CN was treated with 6 M HCl for 96 h, we obtained Co@CN, which was composed of metal Co without cobalt oxide.

Characterization. The Co content was measured by ICP-AES (IRIS Intrepid II XSP, Thermo Fisher Scientific, USA). The Co contents of CoO_x@CN and CoO_x@AC were 29.6% and 27.5%, respectively. Elemental analysis was performed by Elementary Varo MACRO. The content of nitrogen of CoO_x@CN was 1.66%. TEM (Model JEM-1230, JEOL Co. Ltd., Japan) characterization was operated at an accelerating voltage of 80 kV. The diffraction data were collected at room temperature with 2θ scan range between 10° and 80° using a wide-angle X-ray diffraction (Model D/tex-Ultima TV, 1.6 kV, Rig-aku, Japan) equipped with Cu Kα radiation (1.54 Å). The X-ray photoelectron spectra were obtained with an ESCALAB MARK II spherical analyzer using a magnesium anode (Mg 1253.6 eV) X-ray source. All XPS spectra were corrected using the C 1s line at 284.5 eV, and curve fitting and background subtraction were accomplished. The scanning electron microscope (SEM) images were obtained with Zeiss Sigma field emission SEM (Model 8100). The Brunauer−Emmett−Teller (BET) surface areas and porous structure of the samples were measured by using micromeritics ASAP 2020 HD88.

Electrochemical Measurements. The electrochemical tests were carried out in a conventional three electrode electrochemical cell by using a CHI750E. The electrochemical impedance spectroscopy (EIS) measurements were carried out by applying Gamry reference 600 instrument. A commercial glassy carbon electrode (GCE, 5 mm diameter, 0.196 cm^2) was served as the working electrode. The presented current density referred to the geometric surface area of the GCE. A saturated calomel electrode (SCE) and Pt plate were used as the reference electrode and the counter electrode, respectively. The preparation of the working electrode was performed as described below: ethanol suspensions containing 500 μL ethanol, 3 mg of catalyst, and 50 μL 5 wt % Nafion solutions were obtained by ultrasonic mixing for about 30 min. The 15 μL of the catalyst ink suspension thus obtained was coated onto the polished GC electrode, and then it was left to dry in air (this gave a catalyst loading of ∼0.42 mg cm^{-2} and metal loading of ∼0.12 mg cm^{-2} on the GCE). For alkaline electrolytic cell, foam Ni (1 × 1 cm) was utilized as working electrode to reach a high catalyst loading. Eight mg catalyst and 1 mL polytetrafluoroethylene ethanol dispersion solution (1 mg mL^{-1}) were mixed well by ultrasonicating for 20 min. Then, the uniform suspension was dropped on foam Ni and left to dry in infrared lamp (this yielded an approximate metal loading of ∼2.1 mg cm^{-2} on Ni foam). The potential, measured against a SCE electrode, was converted to the potential versus the reversible hydrogen electrode (RHE) according to $E_{vs\ RHE} = E_{vs\ SCE} + E^{\theta}_{\ SCE} + 0.059$ pH. Electrochemical measurements of catalysts were measured in 1 M KOH solution (pH = 14) after purging the electrolyte with N_2 gas for 30 min at 25 °C. To compare the influence of the structure and component of catalysts to HER and OER activities, the electrocatalytic activities of other catalysts were measured under similar conditions, and the corresponding electrocatalytic results are included in the main text.

RESULTS AND DISCUSSION

As illustrated in Scheme S1, the synthesis of CoO_x@CN was achieved by simple thermal treatment of the inexpensive starting materials (Melamine, $CoNO_3{\cdot}6H_2O$ and D(+)-glucosamin hydrochloride) at 800 °C in N_2 atmosphere. The flake-like morphology of the resulting hybrids is observed in the SEM image (Figure 1a) and the TEM image (Figure 1b). Since melamine can form sheets[65,66] by thermal decomposition, the production of cobalt−cobalt oxide/N-doped carbon sheets may arise from melamine. The TEM image of CoO_x@CN in Figure 1b indicates the formed cobalt NPs are uniformly dispersed on N-doped carbon sheets. The size distribution histogram in the inset of Figure 1b demonstrates that these CoO_x NPs have average size of 12.3 nm. The high-resolution (HR) TEM image in Figure 1c clearly reveals that lattice fringe spaces of 2.89 and 4.68 Å are consistent with the (220) and (111) plane of cubic Co_3O_4 spinel-phase, respectively, and also uncovers the resolved lattice fringes of CoO (111) planes with a spacing of 2.47 Å. Metallic cobalt NPs with interplanar distance of 2.05 Å correspond to (111) plane of Co^0 as indicated in the HRTEM in Figure 1d. It is evident that Co^0 is embedded in N-doped carbon architecture and surrounded by a few graphitic carbon layers, which is favorable to the stability of catalysts.[67] Scanning TEM energy dispersive X-ray spectroscopy (STEM-

DOI: 10.1021/ja5127165
J. Am. Chem. Soc. 2015, 137, 2688−2694

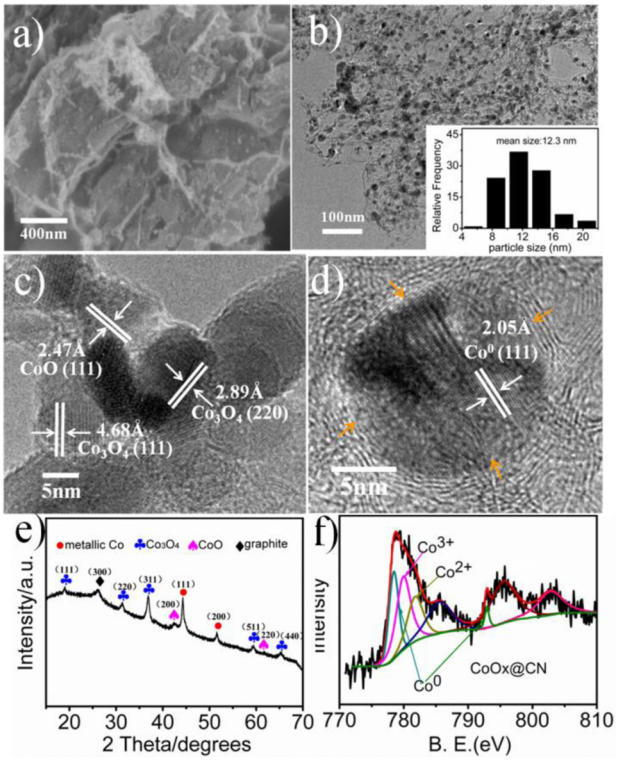

Figure 1. (a) SEM images of CoO_x@CN; (b) TEM image of CoO_x@CN with the inset showing the corresponding particle-size distribution histogram; (c) HRTEM image of Co_3O_4 and CoO on CN; (d) HRTEM image of metallic Co embedded in CN (the pointed parts by arrows represent the graphitic carbon layers); (e) XRD patterns; and (f) high-resolution deconvoluted Co_{2p} spectrum (Co^0, Co^{2+}, and Co^{3+}) of CoO_x@CN.

EDS) elemental mapping was employed to obtain elemental distribution of Co, C, N, and O in the hybrids (Figure S1a–e), verifying the uniform dispersion of four elements. CoO_x@CN was further characterized by the power X-ray diffraction (XRD) patterns in Figure 1e. The diffraction peak at 26.1° suggests the formation of graphitic carbon during the pyrolysis. The peaks at 19.06°, 31.27°, 36.9°, 59.5°, and 65.4° can be ascribed to Co_3O_4, and the peaks at 42.5° and 61.8° are assigned to CoO, with 44.3° and 51.5° belonging to Co^0, which coincides with the HRTEM image, both indicating the existence of Co_3O_4, CoO, and Co^0. Furthermore, the presence of cobalt oxide and metallic cobalt is also confirmed by X-ray photoelectron spectroscopy (XPS) (Figure 1f). As manifested in Figure 1f, the two core-level signals of Co in CoO_x@CN located at ~780 and 796 eV are attributed to $Co_{2p3/2}$ and $Co_{2p1/2}$, respectively. After deconvolution, the peaks around 780 and 795.7 eV are assigned to Co_3O_4 phase, while those around 778.5 and 793.0 eV corresponding to Co^0. Integral data show the ratio of Co^{3+}/Co^{2+} is 1.78, and Co^0 occupies 15.2%. The N_{1s} spectrum of CoO_x@CN in Figure S2 can be deconvoluted into five types of nitrogen species, which are attributed to pyridinic, pyrollic, quaternary, oxidized, and chemisorbed nitrogen atoms according to their binding energies. All of these observations manifest that cobalt–cobalt oxide/N-doped carbon hybrids have been prepared successfully through one-pot annealing method.

The electrocatalytic activity of CoO_x@CN for HER on a GCE was evaluated in 1 M KOH solution using a typical three electrode system. Polarization curves were obtained from linear sweep voltammetry (LSV) measurements with a sweep rate of 5 mV s^{-1}. All HER and OER data have been corrected based on impedance spectroscopy. Compared to the original data, the variation of the IR-corrected data for CoO_x@CN toward HER is evident as seen in Figure S3. In Figure 2a, CoO_x@CN

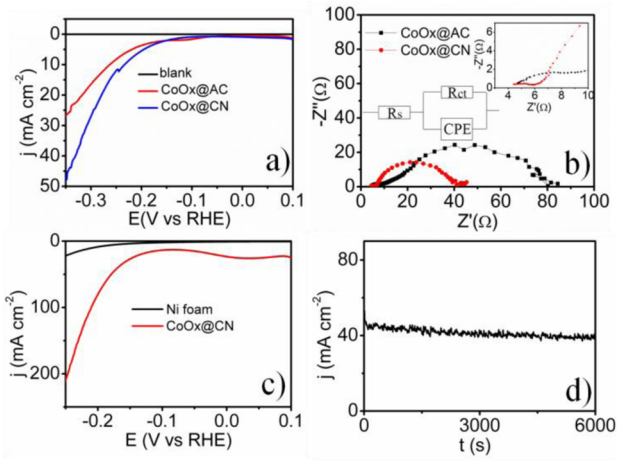

Figure 2. (a) LSV curves and (b) Nyquist plots (overpotential = 250 mV) of CoO_x@CN and CoO_x@AC on GCE; (c) LSV curves of CoO_x@CN on Ni foam; and (d) time dependence of the current density under a constant overpotential of 350 mV of CoO_x@CN. (All tests are for HER.)

exhibits a small onset potential (Figure S4) of 85 mV vs RHE and achieves current density of 10 mA cm^{-2} at overpotential of 232 mV, whereas CoO_x@AC demands 270 mV overpotential to reach a current density of 10 mA cm^{-2}. These values for CoO_x@CN are superior to the behavior of other non-noble-metal HER catalysts in alkaline media, such as amorphous MoS_x,[19] Ni,[68] MnNi, Co-NRCNTs,[38] $NiMoN_x$/C,[26] MoO_3-MoS_2,[20] etc. (Table S1). Moreover, the overpotential of 232 mV is comparable to the activity of MoB[23] and MoC[69,70] (Table S1). As blank control group, bare GCE shows almost no HER performance. Figure S5 presents the optical photograph of the obvious hydrogen bubbles generated on the CoO_x@CN catalyst modified on GCE during the current–time measurements, revealing the production of many hydrogen bubbles on GCE. The influence of different loadings for CoO_x@CN on HER activity is also investigated. As expected, higher loadings for CoO_x@CN result in a better performance for hydrogen production (Figure S6). However, the catalysts cannot perform even better when the metal loading weight overtakes 0.12 mg cm^{-2} due to partial covered active sites (Figure S6).

To investigate the electrode kinetics under HER process, the EIS measurements were carried out from 100 MHz to 0.01 Hz at an overpotential of 250 mV. The semicircles in the high- and low-frequency range of the Nyquist plot attributed to the charge-transfer resistance R_{CT} and solution resistance R_S, respectively, are related to the electrocatalytic kinetics and a lower value corresponds to a faster reaction rate.[71] Similarly, smaller R_{CT} of 41 Ω is realized on CoO_x@CN compared to CoO_x@AC (85 Ω), consistent with the lower overpotential. The superior activity of CoO_x@CN to CoO_x@AC for HER in alkaline media may arise from the bigger pore diameter which could yield easier mass transportation[72,73] (Figure S7 and Table S2). When CoO_x@CN is supported on Ni foam with a loading weight of 2.1 mg cm^{-2}, it presents a small overpotential of 134 mV to reach an current density of 20 mA cm^{-2} and shows a

DOI: 10.1021/ja5127165
J. Am. Chem. Soc. 2015, 137, 2688–2694

large cathode current density of 83 mA cm^{-2} at η = 200 mV, which is about 12 times that of pure commercial Ni foam (7 mA cm^{-2}) applied as industrial alkaline water electrolysis[36,74] in 1 M KOH in Figure 2c. Furthermore, CoO_x@CN exhibits a considerable overpotential of 280 mV at 10 mA cm^{-2} even in neutral solution (Figure S8). Besides the HER activity, stability is another significant criterion to evaluate an advanced electrocatalyst.[75] To probe the durability of CoO_x@CN under media condition, continuous HER at static overpotential was conducted. As shown in Figure 2d, the as-measured time-dependent curve at an overpotential of 350 mV is in typical serrate shape due to the alternate processes of bubble accumulation and bubble release.[76] The current density exhibits negligible degradation even after a long period of 6000 s. The retained activity of CoO_x@CN is ascribed to the protected Co^0 which embedded in carbon architecture, meanwhile, the slight degradation of activity may derive from the consumption of OH^- or the variation of valence state of CoO_x.[77]

To compare the influence of the structure and component of catalysts to HER activity, different component materials (Co@CN, CoO_x@C, and CN) were prepared, and their catalytic properties were also investigated detailly. The characteristic peaks of Co^0 can only be observed from the XRD pattern of Co@CN (Figure 3a, red line), indicating most of cobalt oxide

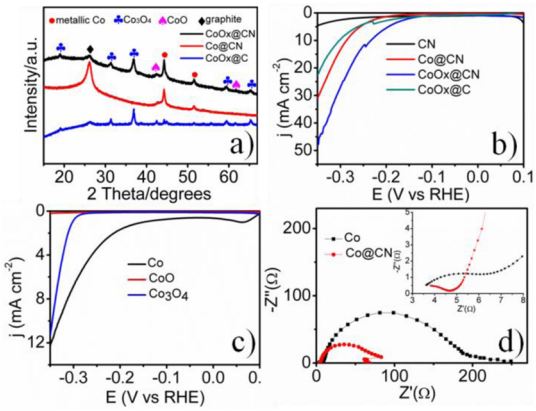

Figure 3. (a) XRD patterns of CoO_x@CN, Co@CN, and CoO_x@C; (b) and (c) LSV curves of different catalysts; (d) Nyquist plots of Co and Co@CN (overpotential = 250 mV). (All tests are for HER.)

has been removed by acid and the carbon-encapsulated Co^0 is reserved. CoO_x@CN consists of nitrogen-doped carbon, metallic cobalt, and cobalt oxide, so which component is the active site or plays a leading role? CoO_x@CN demonstrates the best catalytic performance for HER among four catalysts as shown in Figure 3b. Co@CN mainly including Co^0 presents excellent activity toward HER, revealing the pivotal effect of Co^0 as active sites.[67] CoO_x@CN including Co^0, CoO, and Co_3O_4 obviously outperforms Co@CN with little CoO and Co_3O_4, making it clear that cobalt oxide also plays some degree of catalytic role for HER. Moreover, Co^0 and Co_3O_4 exhibit remarkably larger cathode current density for HER than CoO in Figure 3c, further verifying the catalytic effect of Co^0 and Co_3O_4 as active species toward HER. Therefore, we tentatively propose that metal Co and cobalt oxide may be synergistic active sites for HER catalysis based on the above results. The HER process could be through the Volmer–Tafel process or Volmer–Heyrovsky pathway in basic media.[78]

$$H_2O + e^- \rightarrow H_{ads} + OH^- \text{ (Volmer)}$$
$$H_{ads} + H_{ads} \rightarrow H_2 \text{ (Tafel)} \quad (1)$$

$$H_2O + e^- \rightarrow H_{ads} + OH^- \text{ (Volmer)}$$
$$H_{ads} + H_2O + e^- \rightarrow H_2 + OH^- \text{ (Heyrovsky)} \quad (2)$$

Both pathways involve the adsorption of H_2O molecule, the dissociation of adsorbed H_2O into adsorbed H atom and OH^-, desorption of OH^- to refresh the surface, and the transformation of adsorbed H into H_2. As previously reported, Co metal has been calculated to have a proper binding energy for H atom (close to Pt),[35,36,79] and CoO and Co_3O_4 can be hydroxylated to dissociation water.[80,81] Thus, in our hybrids-CoOx@CN composed of Co^0, CoO, and Co_3O_4, the OH^- generated by H_2O decomposition could preferentially attach to CoO and Co_3O_4 surface due to strong electrostatic affinity to the locally positively charged Co^{2+} and Co^{3+} species, while a nearby Co site would facilitate H adsorption, completing the Volmer process and imparting the synergistic effect to metal Co and cobalt oxide for HER. The Tafel test of CoO_x@CN was conducted in 1 M KOH solution. As shown in Figure S4, the resulting Tafel plot is fit to the Tafel equation ($\eta = b \log j + a$), where j is the current density and b is the Tafel slope), yielding a Tafel slope of 115 mV dec^{-1} for CoO_x@CN. The mechanism of hydrogen evolution in basic solution is not fully clear, but the Tafel slope of CoO_x@CN under basic conditions reveals that the HER may be controlled by a Volmer–Heyrovsky mechanism because the Tafel slope is practically identical to that for smooth Ni (ca. 120 mV dec^{-1}).[82]

CN without cobalt oxide exhibits the negligible activity for HER, implying that CN may be not the active site for HER. However, the conductivity and large surface area of CN for the contribution to HER are not overlooked. First, the pure metal Co produces larger charge-transfer resistance (200 Ω) than Co@CN (85 Ω) in Figure 3d, indicating the intrinsic high conductive carbon facilitates the fast electron transfer.[83] Besides that, the accumulation of cobalt oxide supported on nitrogen-doped carbon with large surface area is avoided, and Co NPs are distributed on CN uniformly, producing more exposured active sites to HER. As indicated in Figure S9, CoO_x@CN has a large double-layer capacitance (37.4 mF cm^{-2}).[84] Finally, the protected Co NPs incorporated in carbon structure sustain the stability of CoO_x@CN for HER (Figure 1d, Figure 2d). Moreover, CoO_x@CN with nitrogen presents obviously higher activity for HER compared to CoO_x@C (non-nitrogen) in Figure 3b, hence the effect of nitrogen is also further investigated. As shown in the XRD pattern of Figure 3a, the diffraction peaks of Co^0 are almost invisible, and more characteristic peaks of Co_3O_4 occur in the nitrogen-free catalyst-CoO_x@C. In contrast, the diffraction peaks of Co^0 in CoO_x@CN are highly evident, suggesting that the incorporation of nitrogen is beneficial to the reduction of Co^{2+} to Co^0 due to the electron-donating effect of nitrogen.[85,86] Hence, the preferable catalytic activity of CoO_x@CN to CoO_x@C may originate from the introduction of nitrogen by increasing the percentage of Co^0, again confirming the crucial role of Co^0 served as catalytic species toward HER in basic solution.

In general, the above discussions indicate that the remarkable catalytic performance of CoO_x@CN could be attributed to the synergistic effect of metal Co and cobalt oxide, high conductive and large surface area carbon, and electron-rich nitrogen.

DOI: 10.1021/ja5127165
J. Am. Chem. Soc. 2015, 137, 2688–2694

The catalytic ability of CoO_x@CN to oxygen evolution reaction was also assessed in 1 M KOH solution. The OER catalytic performance of CoO_x@CN was first examined by linear scan voltammograms. As shown in Figure 4a, the CoO_x@CN supported on Ni foam requires overpotential of 0.26 V for a current density of 10 mA cm^{-2}, which is comparable and even superior to Co_3O_4/N-rmGO,[60] NG-NiCo,[62] $Zn_xCo_{3-x}O_4$,[47] N-CG-CoO,[46] etc. (Table S3). Furthermore, CoO_x@CN only requires a small overpotential of 0.30 V to reach a current density of 10 mA cm^{-2} even in neutral solution in Figure S10. As observed in Figure 4b, when CoO_x@CN loaded on GCE, its catalytic activity compares favorably to the behavior of pure Co_3O_4. Impressively, the R-CoO_x@CN (CoO_x@CN after half an hour HER) exhibits a significant larger current density than CoO_x@CN. In addition, the catalytic performance of R-CoO_x@CN for oxygen evolution exceeds CoO_x@CN even after 1600 s as observed in Figure 4c. The reasons for the enhanced electrocatalytic activity of R-CoO_x@CN relative to CoO_x@CN are elaborated. The Co_{2p} XPS spectrum of R-CoO_x@CN (Figure S11a and Table S4) shows the bigger ratio of Co^{3+}/Co^{2+} than CoO_x@CN. In other words, the percentage of Co^{2+} in R-CoO_x@CN increases after HER, concluding that the relatively higher Co^{2+} yields the better catalytic ability to OER. Therefore, with the increase of the ratio of Co^{3+}/Co^{2+}, the activity of CoO_x@CN for OER decreases slowly, as indicated in Figure 4c. The notably improved catalytic performance of CoO including Co^{2+} for OER in comparison to Co_3O_4 and Co further confirms that the preferable catalytic efficiency of R-CoO_x@CN arises from the increased Co^{2+} (Figure 4d). Similarly, in Figure S11b and Table S4, the percentage of Co^{3+} in O-CoO_x@CN (CoO_x@CN after 30 min OER) raises after continuously generating oxygen due to the partial oxidation of Co^{2+}.

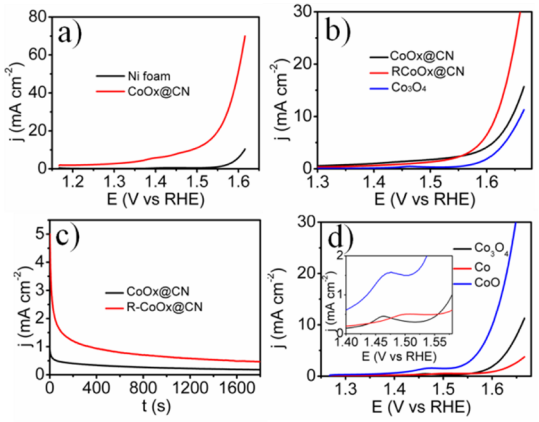

Figure 4. LSV curves of (a) CoO_x@CN supported on Ni foam and (b) CoO_x@CN, R-CoO_x@CN (CoO_x@CN after 30 min HER) and Co_3O_4 loaded on GCE; (c) time dependence of the current density of CoO_x@CN and R-CoO_x@CN under a constant overpotential of 0.35 V; (d) linear sweep curves of Co^0, CoO and Co_3O_4. (All tests are for OER).

Based on the above explanations, we could safely deduce that CoO_x@CN hybrids are highly efficient, non-noble metal-based bifunctional electrocatalysts for HER and OER in alkaline media. Accordingly, we make an electrolyzer with 1 M KOH solution as media by applying CoO_x@CN as the water reduction catalyst and R-CoO_x@CN as the water oxidation catalyst. Water electrolysis with current density of 20 mA cm^{-2} at 1.55 V, comparable to water electrolysis NiO/Ni-CNT and NiFe LDH cell,[78] is observed at room temperature (Figure 5a),

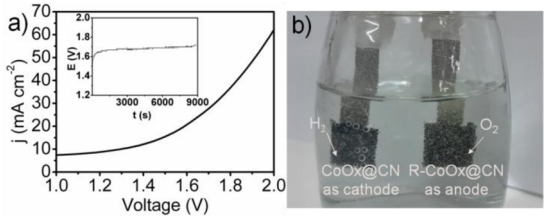

Figure 5. (a) LSV of water electrolysis using original CoO_x@CN as HER catalyst and CoO_x@CN after HER as OER catalyst (both loaded into Ni foam at a loading of 2 mg cm^{-2} based on the active mass) in 1 M KOH, with the inset showing the stability test of electrolyzer at 10 mA cm^{-2}. (b) Optical photograph showing the generation of hydrogen and oxygen bubbles on Ni foam.

and the obvious hydrogen and oxygen bubbles form on Ni foam (Figure 5b). Stability is an important criterion to evaluate an electrolytic cell. The durability of electrolyzer was carried out at 10 mA cm^{-2} in 1 M KOH solution at 25 °C. As observed in the inset of Figure 5a, the cell exhibits considerable stability in nearly 3 h. Notably, there are few reports about splitting water into H_2 and O_2 using a nonprecious catalyst with different valence state metals as anode and cathode, which paves a new pathway for designing overall water splitting catalysts.

CONCLUSIONS

In conclusion, cobalt−cobalt oxide/N-doped carbon sheets hybrids (CoO_x@CN) have been synthesized successfully through easily scalable and cost-effective one-pot annealing method. CoO_x@CN exhibited superior bifunctional catalytic efficiency for HER and OER. The excellent HER catalytic ability of CoO_x@CN hybrids could be attributed to the following four reasons: (1) the uniformly distributed Co NPs supported on high surface area carbon enabled the full use of active sites of catalyst, and the high conductivity of carbon was favorable to the transfer of electron; (2) the protected carbon-encapsulated Co NPs sustained the stability; (3) the synergistic effect of metallic cobalt and cobalt oxide; and (4) the incorporation of nitrogen into carbon architecture improved the catalytic activity by increasing the proportion of Co^0 due to the electron-donating effects. The improved catalytic ability of CoO_x@CN after HER toward OER arose from the improved percentage of Co^{2+}. When applied as water electrolysis catalyst, CoO_x@CN reached a current density of 20 mA cm^{-2} at 1.55 V. It is scarcely reported that splitting water into H_2 and O_2 using a nonprecious catalyst with different valence state metals as anode and cathode, which encouraged us to explore overall water splitting catalysts.

ASSOCIATED CONTENT

Supporting Information

The synthesis process of CoO_x@CN in Scheme S1, STEM-EDS elemental maps of CoO_x@CN, high-resolution deconvoluted N 1s and Co_{2p} spectrum, double-layer capacitance measurements, Tafel plots, and the comparison of the electrocatalytic activity of CoO_x@CN to recently reported catalysts for HER and OER in basic solutions. This material is available free of charge via the Internet at http://pubs.acs.org.

DOI: 10.1021/ja5127165
J. Am. Chem. Soc. 2015, 137, 2688−2694

AUTHOR INFORMATION

Corresponding Author

*chemwy@zju.edu.cn

Notes

The authors declare no competing financial interest.

ACKNOWLEDGMENTS

This work was supported by the National Natural Science Foundation of China (21376208 and J1210042), the Zhejiang Provincial Natural Science Foundation for Distinguished Young Scholars of China (LR13B030001), the Specialized Research Fund for the Doctoral Program of Higher Education (J20130060), the Fundamental Research Funds for the Central Universities, the Program for Zhejiang Leading Team of S&T Innovation, the Fundamental Research Funds for the Central Universities, and the Partner Group Program of the Zhejiang University and the Max-Planck Society are greatly appreciated.

REFERENCES

(1) Bloor, L. G.; Molina, P. I.; Symes, M. D.; Cronin, L. *J. Am. Chem. Soc.* **2014**, *136*, 3304.
(2) Maeda, K.; Teramura, K.; Lu, D. L.; Takata, T.; Saito, N.; Inoue, Y.; Domen, K. *Nature* **2006**, *440*, 295.
(3) Park, S.; Shao, Y.; Liu, J.; Wang, Y. *Energy Environ. Sci.* **2012**, *5*, 9331.
(4) Chen, S.; Qiao, S.-Z. *ACS Nano* **2013**, *7*, 10190.
(5) Meyer, T. J. *Nature* **2008**, *451*, 778.
(6) Jiao, F.; Frei, H. *Angew. Chem., Int. Ed.* **2009**, *48*, 1841.
(7) Robinson, D. M.; Go, Y. B.; Mui, M.; Gardner, G.; Zhang, Z.; Mastrogiovanni, D.; Garfunkel, E.; Li, J.; Greenblatt, M.; Dismukes, G. C. *J. Am. Chem. Soc.* **2013**, *135*, 3494.
(8) Seitz, L. C.; Chen, Z.; Forman, A. J.; Pinaud, B. A.; Benck, J. D.; Jaramillo, T. F. *ChemSusChem* **2014**, *7*, 1372.
(9) Zhang, M.; de Respinis, M.; Frei, H. *Nat. Chem.* **2014**, *6*, 362.
(10) Trotochaud, L.; Ranney, J. K.; Williams, K. N.; Boettcher, S. W. *J. Am. Chem. Soc.* **2012**, *134*, 17253.
(11) Shiraishi, Y.; Kofuji, Y.; Kanazawa, S.; Sakamoto, H.; Ichikawa, S.; Tanaka, S.; Hirai, T. *Chem. Commun.* **2014**, *50*, 15255.
(12) Bai, S.; Wang, C.; Deng, M.; Gong, M.; Bai, Y.; Jiang, J.; Xiong, Y. *Angew. Chem., Int. Ed.* **2014**, *53*, 12120.
(13) Shim, Y.; Young, R. M.; Douvalis, A. P.; Dyar, S. M.; Yuhas, B. D.; Bakas, T.; Wasielewski, M. R.; Kanatzidis, M. G. *J. Am. Chem. Soc.* **2014**, *136*, 13371.
(14) Das, R. K.; Wang, Y.; Vasilyeva, S. V.; Donoghue, E.; Pucher, I.; Kamenov, G.; Cheng, H.-P.; Rinzler, A. G. *ACS Nano* **2014**, *8*, 8447.
(15) Sathe, B. R.; Zou, X.; Asefa, T. *Catal. Sci. Technol.* **2014**, *4*, 2023.
(16) Yan, Y.; Ge, X.; Liu, Z.; Wang, J.-Y.; Lee, J.-M.; Wang, X. *Nanoscale* **2013**, *5*, 7768.
(17) Yan, Y.; Xia, B.; Xu, Z.; Wang, X. *ACS Catal.* **2014**, *4*, 1693.
(18) Hinnemann, B.; Moses, P. G.; Bonde, J.; Jørgensen, K. P.; Nielsen, J. H.; Horch, S.; Chorkendorff, I.; Nørskov, J. K. *J. Am. Chem. Soc.* **2005**, *127*, 5308.
(19) Merki, D.; Fierro, S.; Vrubel, H.; Hu, X. *Chem. Sci.* **2011**, *2*, 1262.
(20) Chen, Z.; Cummins, D.; Reinecke, B. N.; Clark, E.; Sunkara, M. K.; Jaramillo, T. F. *Nano Lett.* **2011**, *11*, 4168.
(21) Kibsgaard, J.; Jaramillo, T. F.; Besenbacher, F. *Nat. Chem.* **2014**, *6*, 248.
(22) Vrubel, H.; Hu, X. *Angew. Chem., Int. Ed.* **2012**, *51*, 12703.
(23) Wan, C.; Regmi, Y. N.; Leonard, B. M. *Angew. Chem., Int. Ed.* **2014**, *53*, 6407.
(24) Xiao, P.; Yan, Y.; Ge, X.; Liu, Z.; Wang, J.-Y.; Wang, X. *Appl. Catal., B* **2014**, *154*−*155*, 232.
(25) Lukowski, M. A.; Daniel, A. S.; English, C. R.; Meng, F.; Forticaux, A.; Hamers, R. J.; Jin, S. *Energy Environ. Sci.* **2014**, *7*, 2608.
(26) Chen, W. F.; Sasaki, K.; Ma, C.; Frenkel, A. I.; Marinkovic, N.; Muckerman, J. T.; Zhu, Y.; Adzic, R. R. *Angew. Chem., Int. Ed.* **2012**, *51*, 6131.
(27) Shalom, M.; Gimenez, S.; Schipper, F.; Herraiz-Cardona, I.; Bisquert, J.; Antonietti, M. *Angew. Chem., Int. Ed.* **2014**, *53*, 3654.
(28) Zheng, Y.; Jiao, Y.; Zhu, Y.; Li, L. H.; Han, Y.; Chen, Y.; Du, A.; Jaroniec, M.; Qiao, S. Z. *Nat. Commun.* **2014**, *5*, 3783.
(29) Zeng, K.; Zhang, D. *Prog. Energy Combust. Sci.* **2010**, *36*, 307.
(30) Hall, D. E. *J. Electrochem. Soc.* **1981**, *128*, 740.
(31) McArthur, M. A.; Jorge, L.; Coulombe, S.; Omanovic, S. *J. Power Sources* **2014**, *266*, 365.
(32) McCrory, C. C.; Jung, S.; Peters, J. C.; Jaramillo, T. F. *J. Am. Chem. Soc.* **2013**, *135*, 16977.
(33) Zhao, Y.; Nakamura, R.; Kamiya, K.; Nakanishi, S.; Hashimoto, K. *Nat. Commun.* **2013**, *4*, 2390.
(34) Lin, C.-H.; Chen, C.-L.; Wang, J.-H. *J. Phys. Chem. C* **2011**, *115*, 18582.
(35) Yao Zheng, Y. J.; Jaroniec, Mietek; Shi Zhang, Qiao *Angew. Chem., Int. Ed.* **2014**, *53*, 2.
(36) Lupi, C.; Dell'Era, A.; Pasquali, M. *Int. J. Hydrogen Energy* **2009**, *34*, 2101.
(37) Zheng, Y.; Jiao, Y.; Jaroniec, M.; Qiao, S. Z. *Angew. Chem., Int. Ed.* **2015**, *54*, 52.
(38) Zou, X.; Huang, X.; Goswami, A.; Silva, R.; Sathe, B. R.; Mikmekova, E.; Asefa, T. *Angew. Chem., Int. Ed.* **2014**, *53*, 4372.
(39) Artero, V.; Chavarot-Kerlidou, M.; Fontecave, M. *Angew. Chem., Int. Ed.* **2011**, *50*, 7238.
(40) Lei, H.; Han, A.; Li, F.; Zhang, M.; Han, Y.; Du, P.; Lai, W.; Cao, R. *Phys. Chem. Chem. Phys.* **2014**, *16*, 1883.
(41) Li, Y.; Malik, M. A.; O'Brien, P. *J. Am. Chem. Soc.* **2005**, *127*, 16020.
(42) Ahn, H. S.; Davenport, T. C.; Tilley, T. D. *Chem. Commun.* **2014**, *50*, 3834.
(43) Zhao, J.; Zou, Y.; Zou, X.; Bai, T.; Liu, Y.; Gao, R.; Wang, D.; Li, G. D. *Nanoscale* **2014**, *6*, 7255.
(44) Liang, Y.; Li, Y.; Wang, H.; Zhou, J.; Wang, J.; Regier, T.; Dai, H. *Nat. Mater.* **2011**, *10*, 780.
(45) Zou, X.; Goswami, A.; Asefa, T. *J. Am. Chem. Soc.* **2013**, *135*, 17242.
(46) Mao, S.; Wen, Z.; Huang, T.; Hou, Y.; Chen, J. *Energy Environ. Sci.* **2014**, *7*, 609.
(47) Liu, X.; Chang, Z.; Luo, L.; Xu, T.; Lei, X.; Liu, J.; Sun, X. *Chem. Mater.* **2014**, *26*, 1889.
(48) Ma, T. Y.; Dai, S.; Jaroniec, M.; Qiao, S. Z. *J. Am. Chem. Soc.* **2014**, *136*, 13925.
(49) Esswein, A. J.; McMurdo, M. J.; Ross, P. N.; Bell, A. T.; Tilley, T. D. *J. Phys. Chem. C* **2009**, *113*, 15068.
(50) Zhao, J.; Zou, Y.; Zou, X.; Bai, T.; Liu, Y.; Gao, R.; Wang, D.; Li, G.-D. *Nanoscale* **2014**, *6*, 7255.
(51) Tueysuez, H.; Hwang, Y. J.; Khan, S. B.; Asiri, A. M.; Yang, P. *Nano Res.* **2013**, *6*, 47.
(52) Koza, J. A.; He, Z.; Miller, A. S.; Switzer, J. A. *Chem. Mater.* **2012**, *24*, 3567.
(53) Chae, H. K.; Siberio-Perez, D. Y.; Kim, J.; Go, Y.; Eddaoudi, M.; Matzger, A. J.; O'Keeffe, M.; Yaghi, O. M. *Nature* **2004**, *427*, 523.
(54) Chen, S.; Bi, J.; Zhao, Y.; Yang, L.; Zhang, C.; Ma, Y.; Wu, Q.; Wang, X.; Hu, Z. *Adv. Mater.* **2012**, *24*, 5593.
(55) Ryoo, R.; Joo, S. H.; Kruk, M.; Jaroniec, M. *Adv. Mater.* **2001**, *13*, 677.
(56) Dai, L.; Chang, D. W.; Baek, J.-B.; Lu, W. *Small* **2012**, *8*, 1130.
(57) Wang, Y.; Zhang, H. J.; Lu, L.; Stubbs, L. P.; Wong, C. C.; Lin, J. *ACS Nano* **2010**, *4*, 4753.
(58) Shi, P.; Su, R.; Wan, F.; Zhu, M.; Li, D.; Xu, S. *Appl. Catal., B* **2012**, *123*, 265.
(59) Ma, T. Y.; Dai, S.; Jaroniec, M.; Qiao, S. Z. *J. Am. Chem. Soc.* **2014**, *136*, 13925.
(60) Liang, Y.; Li, Y.; Wang, H.; Zhou, J.; Wang, J.; Regier, T.; Dai, H. *Nat. Mater.* **2011**, *10*, 780.

DOI: 10.1021/ja5127165
J. Am. Chem. Soc. 2015, 137, 2688−2694

(61) Zou, X.; Goswami, A.; Asefa, T. *J. Am. Chem. Soc.* **2013**, *135*, 17242.
(62) Chen, S.; Duan, J.; Jaroniec, M.; Qiao, S. Z. *Angew. Chem., Int. Ed.* **2013**, *52*, 13567.
(63) Cobo, S.; Heidkamp, J.; Jacques, P.-A.; Fize, J.; Fourmond, V.; Guetaz, L.; Jousselme, B.; Ivanova, V.; Dau, H.; Palacin, S.; Fontecave, M.; Artero, V. *Nat. Mater.* **2012**, *11*, 802.
(64) Zhang, C.; Antonietti, M.; Fellinger, T.-P. *Adv. Funct. Mater.* **2014**, *24*, 7655.
(65) Terrones, M.; Redlich, P.; Grobert, N.; Trasobares, S.; Hsu, W. K.; Terrones, H.; Zhu, Y. Q.; Hare, J. P.; Reeves, C. L.; Cheetham, A. K.; Ruhle, M.; Kroto, H. W.; Walton, D. R. M. *Adv. Mater.* **1999**, *11*, 655.
(66) Doblinger, M.; Lotsch, B. V.; Wack, J.; Thun, J.; Senker, J.; Schnick, W. *Chem. Commun.* **2009**, 1541.
(67) Deng, J.; Ren, P.; Deng, D.; Yu, L.; Yang, F.; Bao, X. *Energy Environ. Sci.* **2014**, *7*, 1919.
(68) Kirk, D. W.; Thorpe, S. J.; Suzuki, H. *Int. J. Hydrogen Energy* **1997**, *22*, 493.
(69) Ledendecker, M.; Clavel, G.; Antonietti, M.; Shalom, M. *Adv. Funct. Mater.* **2015**, *25*, 393.
(70) Liao, L.; Wang, S.; Xiao, J.; Bian, X.; Zhang, Y.; Scanlon, M. D.; Hu, X.; Tang, Y.; Liu, B.; Girault, H. H. *Energy Environ. Sci.* **2014**, *7*, 387.
(71) Xie, J.; Zhang, H.; Li, S.; Wang, R.; Sun, X.; Zhou, M.; Zhou, J.; Lou, X. W.; Xie, Y. *Adv. Mater.* **2013**, *25*, 5807.
(72) Jin, H.; Xiong, T.; Li, Y.; Xu, X.; Li, M.; Wang, Y. *Chem. Commun.* **2014**, *50*, 12637.
(73) Kim, S. Y.; Jeong, H. M.; Kwon, J. H.; Ock, I. W.; Suh, W. H.; Stucky, G. D.; Kang, J. K. *Energy Environ. Sci.* **2015**, *8*, 188.
(74) LeRoy, R. L. *Int. J. Hydrogen Energy* **1983**, *8*, 401.
(75) Bai, S.; Wang, L.; Chen, X.; Du, J.; Xiong, Y. *Nano Res.* **2015**, *8*, 175.
(76) Xie, J.; Zhang, J.; Li, S.; Grote, F.; Zhang, X.; Zhang, H.; Wang, R.; Lei, Y.; Pan, B.; Xie, Y. *J. Am. Chem. Soc.* **2013**, *135*, 17881.
(77) Xu, Y.-F.; Gao, M.-R.; Zheng, Y.-R.; Jiang, J.; Yu, S.-H. *Angew. Chem., Int. Ed.* **2013**, *52*, 8546.
(78) Gong, M.; Zhou, W.; Tsai, M.-C.; Zhou, J.; Guan, M.; Lin, M.-C.; Zhang, B.; Hu, Y.; Wang, D.-Y.; Yang, J.; Pennycook, S. J.; Hwang, B.-J.; Dai, H. *Nat. Commun.* **2014**, *5*, 4695.
(79) Sheng, W.; Myint, M.; Chen, J. G.; Yan, Y. *Energy Environ. Sci.* **2013**, *6*, 1509.
(80) Petitto, S. C.; Marsh, E. M.; Carson, G. A.; Langell, M. A. *J. Mol. Catal. A: Chem.* **2008**, *281*, 49.
(81) Xu, X. L.; Li, J. Q. *Surf. Sci.* **2011**, *605*, 1962.
(82) Marceta Kaninski, M. P.; Nikolic, V. M.; Tasic, G. S.; Rakocevic, Z. L. *Int. J. Hydrogen Energy* **2009**, *34*, 703.
(83) Zhu, J.; Shim, B. S.; Di Prima, M.; Kotov, N. A. *J. Am. Chem. Soc.* **2011**, *133*, 7450.
(84) Tian, J.; Liu, Q.; Cheng, N.; Asiri, A. M.; Sun, X. *Angew. Chem., Int. Ed.* **2014**, *53*, 9577.
(85) Li, X.-H.; Antonietti, M. *Chem. Soc. Rev.* **2013**, *42*, 6593.
(86) Xu, X.; Li, Y.; Gong, Y.; Zhang, P.; Li, H.; Wang, Y. *J. Am. Chem. Soc.* **2012**, *134*, 16987.

DOI: 10.1021/ja5127165
J. Am. Chem. Soc. 2015, 137, 2688−2694